Stability and debris in high-brightness liquid-metal-jet-anode microfocus x-ray sources

M. Otendal,[a] T. Tuohimaa, and H. M. Hertz
Biomedical and X-ray Physics, Department of Applied Physics, Royal Institute of Technology/Albanova, SE-106 91 Stockholm, Sweden

(Received 12 May 2006; accepted 2 November 2006; published online 17 January 2007)

We investigate the x-ray spot stability and the debris emission in liquid-metal-jet anode electron-impact x-ray sources operating in the 10–100 W microfocus regime. The x-ray spot size is 15–23 μm in diameter and the electron-beam power density is up to ~210 kW/mm^2, an order of magnitude higher than for conventional microfocus sources. In the power range of the investigation the source is stable in terms of spot size and position. The debris emission rate increases exponentially with the applied electron-beam power but may be reduced by combining larger and faster target jets with smaller e-beam foci and by mitigation schemes. It is concluded that the investigated factors will not limit the performance and function of liquid-metal-jet-anode electron-impact microfocus sources when operating in this high-brightness regime. © *2007 American Institute of Physics*. [DOI: 10.1063/1.2423229]

The vast majority of x-ray investigations in, e.g., medicine, nondestructive testing, and materials science, are performed with compact electron-impact x-ray sources. Such examinations are often limited by the brightness of the source. The x-ray brightness[1] of electron-impact sources is directly proportional to the electron-beam power density, which is limited by the onset of e-beam induced thermal damage to the anode surface[2] since the majority (~99%) of the kinetic energy of the electrons is converted into heat. The power-density capacity of modern x-ray tubes typically ranges from ~1 kW/mm^2 up to a few tens of kW/mm^2. The lower end of the range applies to long exposures with stationary anode sources with macroscopic (>100 μm) x-ray spots, whereas most high-power sources used for medical diagnostics have rotating anodes that can sustain ~10 kW/mm^2 during short exposures (<1 s). Microfocus tubes with spot sizes of about 10–50 μm can operate at slightly higher electron-beam power densities (a few tens of kW/mm^2). However, a significant improvement to these solid-anode systems seems unlikely.[3] Our system is based on a liquid-metal-jet anode, which intrinsically has a much higher power-density capacity (two to three orders of magnitude) than conventional anodes.[4,5] In brief, this is due to two reasons: the potential for higher jet speeds than what is possible for a rotating anode and the regenerative nature of the liquid jet, which makes the requirement of keeping the anode undamaged more relaxed, consequently allowing vaporization of the jet.

In the present paper we investigate factors that influence the performance and function of the source concept when operated in the 10–100 W microfocus mode. We show that the source size and source position are stable and that the debris emission (tin vapor emitted from the electron-beam/tin-jet interaction point) is manageable in this power range. Previously it was speculated that these factors could potentially limit the scalability of the source to the high-power-density regime allowed by the intrinsic properties of the system.[4] The applied power density in the present experiments is above 200 kW/mm^2, i.e., about an order of magnitude higher than for present solid-anode systems and two orders of magnitude higher than in Ref. 4.

Figure 1 shows the experimental arrangement of the liquid-metal-jet x-ray source. A liquid-metal jet consisting of 99.8% tin is injected through a 30 or 50 μm diameter glass capillary nozzle into an evacuated chamber. Jet speeds of up to 60 m/s can be achieved by applying 200 bars of nitrogen

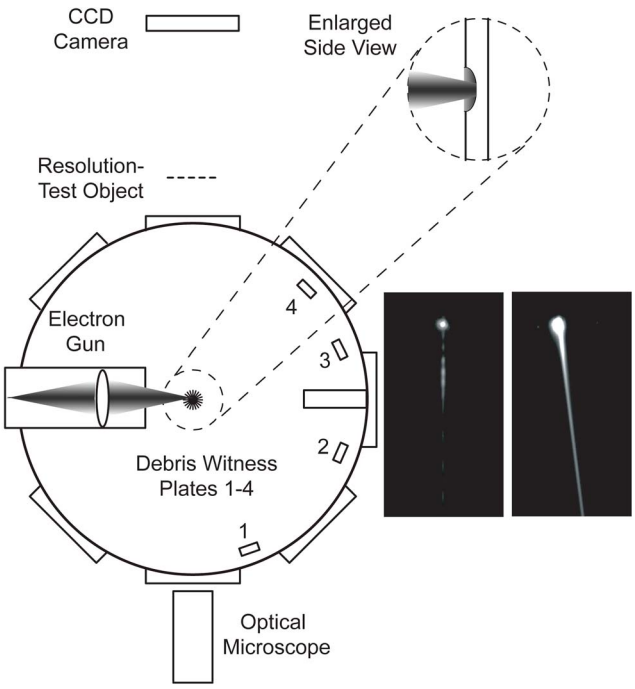

FIG. 1. The experimental arrangement as seen from above. The photo inserts show a liquid-tin jet during low-power (left image) and high-power (right image) operations.

[a]Electronic mail: mikael.otendal@biox.kth.se

pressure over the molten tin. The speed of the target jet is, thus, comparable to the fastest rotating anodes.[6] The electron-beam system is based on a 50 kV LaB_6 cathode electron-beam gun in continuous operation. The e-beam is focused onto the tin jet by a magnetic lens to generate an ~15 or ~23 μm full width at half maximum (FWHM) diameter x-ray spot, where the two spot sizes correspond to two different cathode sizes (50 or 200 μm diameter). The electron gun is pumped with a separate 250 l/s turbo-drag pump, and the apertures at the ends of the magnetic lens are small enough to maintain a sufficient differential pressure between the main vacuum chamber ($\sim 10^{-4}$ mbar) and the electron gun ($\sim 10^{-7}$ mbar). The cathode is shielded from tin vapor by a 1 mm diameter hole in a 120 μm thick aluminum foil, which is placed between the jet and the magnetic lens. The vacuum around the cathode is kept in the low 10^{-7} mbar range even during high-power operation of the gun, resulting in a long lifetime (>1000 h) for the LaB_6 cathode. Debris witness plates are placed at four different positions in the main tank about 150 mm from the x-ray source. For x-ray imaging we use a 4008×2672 pixel phosphor-coated charge coupled device (CCD) detector with 9 μm pixels and a measured point-spread function (PSF) of ~34 μm FWHM. A mammography resolution test object (25 μm wide lines and spaces, 20 μm thick gold) is placed 50 cm from the source and 190 cm in front of the CCD. A 12× zoom microscope is used for optical inspection of the jet.

The first issue to be considered is the stability in size and position of the x-ray spot as a function of electron-beam power and, thus, power density. The source was first optimized by imaging the 20 line pair/mm gold resolution test object on the CCD. By inspecting the visibility of the grating while adjusting the focusing and deflection of the electron beam, the source could be optimized for maximum brightness in real time. The source size was then determined from the imaged intensity profile of a sharp edge in the resolution target. The edge-spread function (ESF) was found by fitting a sum of erf functions to the intensity profile. From the ESF and following Ref. 7, the size of the x-ray spot was determined by calculating the line-spread function (LSF) and the modulation transfer function (MTF) using numerical differentiation and Fourier transformations. The measured x-ray source sizes were also verified by comparing images of the grating-like gold test object with wave propagation simulations. Figure 2 shows the vertical source size (FWHM) as a function of power density with the 200 μm diameter cathode. The measurements include data from 30 and 50 μm diameter jets and jet speeds of 22 and 40 m/s. Independent of power and power density, the vertical source size was 23 ± 1.5 μm. The ± 1.5 μm variation is primarily due to slightly different distances between the magnetic lens and the metal jet for the different experiments. In the horizontal direction an x-ray spot size of 9 ± 2 μm FWHM was measured. The smaller size in the horizontal direction is due to the limited penetration depth of the e-beam into the jet (~4 μm as calculated by a Monte Carlo simulation program[9]), in combination with a slight widening by the curvature of the cylindrical jet and by the experimental difficulty to reproducibly center the electron beam on the jet. A

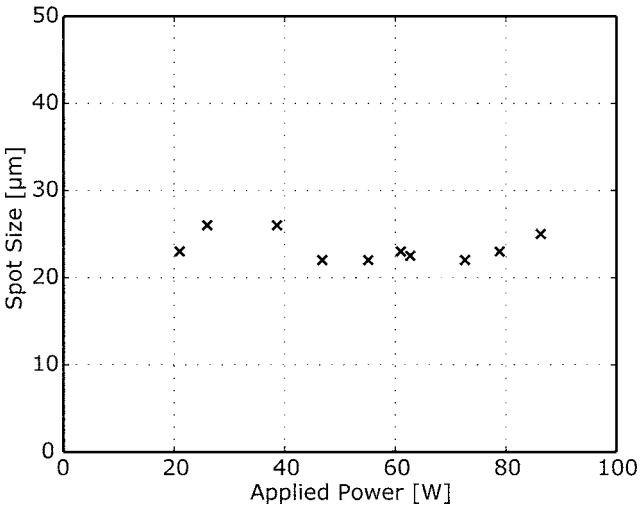

FIG. 2. The x-ray spot size as a function of the applied electron-beam power using the 200 μm cathode.

change to the 50 μm diameter cathode resulted in a vertical spot size of 15 ± 1.5 μm FWHM with a maximum continuous power density of ~210 kW/mm^2 on the metal jet. The horizontal spot size was still in the 9 ± 2 μm range as for the larger cathode. In summary, the source size is constant within the accuracy of the experimental arrangement and the measurements and over the investigated range of power and power density.

When combining high power (80 W) with the small-diameter jet (30 μm), the jet started to tilt at an angle after the interaction point (cf. photo insert in Fig. 1). However, the stability of the size and the position of the x-ray spot were not affected. This angular deflection is due to nonisotropic vapor emission as a result of the asymmetric temperature distribution around the e-beam focus spot on the jet (cf. below). By comparing the tin-vapor deposition on the aluminum foil used for shielding of the cathode and the amount of debris on the witness plates, it was found that the debris emission towards the electron gun was about four times higher than in the forward direction of the e-beam. A simple model based on conservation of momentum for the emitted tin vapor and the bulk of the jet was used to calculate the jet tilt angle. The momentum of the emitted vapor was calculated from the debris measurements, and the model was found to agree well with experimental observations.

Debris emission is a potential practical difficulty. We studied debris deposition rates for a range of different system parameters: an e-beam power between 38 and 86 W, a jet speed of 22 or 40 m/s, a jet diameter of 30 or 50 μm, and an x-ray spot size of ~15 or ~23 μm. The witness plates were exposed to tin vapor for 6–24 min and analyzed with a surface profilometer (KLA Tencor P-15). Figure 3 shows the results. Curve 1 (22 m/s, 30 μm diameter jet, and ~23 μm diameter spot) shows that the debris deposition rate grows exponentially with the power applied on the jet, which is in agreement with the increasing vapor pressure of tin as a function of temperature. The maximum measured debris rate of 0.54 nm/s corresponds to 2 μm/h. Curve 2 depicts the debris emission from a 22 m/s, 50 μm diameter jet with *a*

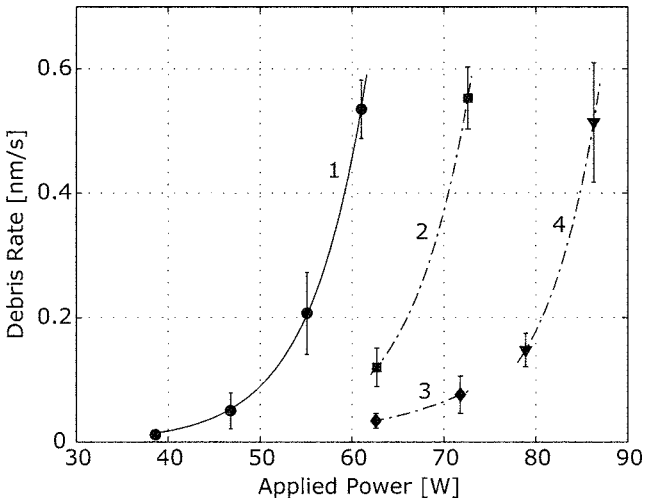

FIG. 3. The debris emission rate at a distance of ~150 mm from the x-ray source as a function of the applied electron-beam power. Curve 1: 22 m/s, 30 μm jet, and 23 μm x-ray spot size. Curve 2: 22 m/s, 50 μm jet, and 23 μm x-ray spot size. Curve 3: 22 m/s, 50 μm jet, and 15 μm x-ray spot size. Curve 4: 40 m/s, 30 μm jet, and 23 μm x-ray spot size. Error bars indicate one standard deviation.

~23 μm spot. By comparing curves 1 and 2 it should be noted that an increased jet diameter leads to a decreased debris emission rate. This is believed to be due to two reasons: (i) the increased mass flow of the larger jet leads to a reduced average temperature of the jet and, thus, a reduced evaporation rate and (ii) increasing the jet diameter, but keeping the size of the electron-beam spot constant, results in a more effective shielding of the very hot electron-beam impact area on the jet in the direction of the debris witness plates. Curve 3 provides further evidence for the shielding concept. Curve 3 has the same jet parameters as curve 2 but the x-ray spot is smaller (~15 μm), which clearly results in improved shielding. At an applied power of 72 W the smaller focus yielded a reduction of the debris emission rate in the direction of the witness plates by a factor of ~16× compared to the ~23 μm spot size operation. Finally, curve 4 shows the impact on the debris rate of an increased target speed (40 m/s, 30 μm diameter jet, and ~23 μm spot). An ~80% increase of the jet velocity in combination with a ~50% increase of the applied power resulted in the same rate of debris emission. Finally, from the experimental data above on debris rates and their angular dependence, we estimate that approximately 1% of the jet is evaporated at ~80 W operation.

From the above we conclude that the liquid-metal-jet anode can be operated with a stable source size and stable position in the 10–100 W microfocus-source range and that the main potential obstacle for the practical utilization of the source is the debris. The debris rates will naturally increase when higher-brightness operation is attempted by increasing the e-beam power and power density. We note that the technological electron-beam power-density limit for subkilowatt LaB_6 electron-beam guns similar to ours is a few tens of MW/mm^2, i.e., two orders of magnitude above the highest power density on the metal-jet anode reported here.[10,11] As mentioned above, the power-density capacity of the liquid-metal-jet anode may generically be improved by increasing the speed of the jet, and it has, in fact, been shown that it should be possible to produce stable tin jets operating at more than 500 m/s.[12] On the other hand, this may not necessarily be the only way to modify the jet for reduced debris production. As is indicated by the results in Fig. 3, a medium-speed jet with a larger diameter may prove to have better debris reduction properties than a considerably faster, but thinner, jet (cf. curves 3 and 4).

For long-term operation and for operation at higher power with correspondingly higher vaporization rates, the source may benefit from a debris mitigation system. The amount of tin-vapor deposition on the x-ray exit window must be controlled to prevent a considerable damping of the x-ray flux. A few possible solutions to this problem, which is shared by the extreme ultraviolet (EUV) lithography community, are plasma windows,[13] foil traps,[14] gas curtains,[15] and the use of a local halogen-containing gas atmosphere.[14]

In summary, we have made a quantitative investigation of the x-ray spot stability and debris emission in liquid-metal-jet-anode x-ray sources. It was found that the size and position of the x-ray spot were stable when operating the source in the in 10–100 W microfocus regime and at high electron-beam power density (~210 kW/mm^2). The debris emission rate increases exponentially with the applied electron-beam power but may be reduced by combining larger and faster target jets with smaller e-beam foci. We conclude that source stability and debris emission are manageable problems and that the source shows good potential to be scaled to even higher e-beam power densities.

This work has been supported by the Swedish Agency for Innovation Systems, the Swedish Foundation for Strategic Research, and the Swedish Research Council.

[1]See, e. g., D. Attwood, *Soft X-Rays and Extreme Ultraviolet Radiation*- (Cambridge University Press, New York, 2000).
[2]*Imaging Systems for Medical Diagnostics*, edited by E. Krestel (Siemens, Berlin, 1990), p. 242.
[3]J. Freudenberger, E. Hell, and W. Knüpfer, Nucl. Instrum. Methods Phys. Res. A **466**, 99 (2001).
[4]O. Hemberg, M. Otendal, and H. M. Hertz, Appl. Phys. Lett. **83**, 1483 (2003).
[5]O. Hemberg, M. Otendal, and H. M. Hertz, Opt. Eng. (Bellingham) **43**, 1682 (2004).
[6]P. Schardt, J. Deuringer, J. Freudenberger, E. Hell, W. Knüpfer, D. Mattern, and M. Schild, Med. Phys. **31**, 2699 (2004).
[7]T. Weitkamp, Ph.D. thesis, Hamburg University, 2002.
[8]T. Tuohimaa, M. Otendal, and H. M. Hertz, Radiology (submitted).
[9]A. R. Couture and D. Drouin, CASINO, 2002, http://www.gel.usherbrooke.ca/casino/.
[10]D. B. Langmuir, Proc. IRE **25**, 8 (1937).
[11]T. Tuohimaa, M. Otendal, H. M. Hertz, Proc. SPIE **5918**, 225 (2005).
[12]M. Otendal, O. Hemberg, T. T. Tuohimaa, and H. M. Hertz, Exp. Fluids **39**, 799 (2005).
[13]A. Hershcovitch and the Acceleron Team, Phys. Plasmas **12**, 57102 (2005).
[14]J. Pankert *et al.*, Proc. SPIE **5751**, 260 (2005).
[15]M. P. Kanouff and A. K. Ray-Chaudhuri, Proc. SPIE **3676**, 735 (1999).